PAPER • OPEN ACCESS

Empirical scaling of the L–H threshold power for metal wall tokamaks using a multi-device database

To cite this article: E. Delabie *et al* 2026 *Nucl. Fusion* **66** 036016

OPEN ACCESS
IOP Publishing | International Atomic Energy Agency
Nuclear Fusion
Nucl. Fusion **66** (2026) 036016 (15pp)
https://doi.org/10.1088/1741-4326/ae39f2

Empirical scaling of the L–H threshold power for metal wall tokamaks using a multi-device database

E. Delabie[1,*], E.R. Solano[2], J.W. Hughes[3], C.F. Maggi[4], F. Ryter[5], G. Birkenmeier[5,6], P. Carvalho[4,7], M. Cavedon[5,8], M. Chernyshova[9], P. David[5], J. Hillesheim[4,10], U. Plank[5], the EUROfusion Tokamak Exploitation Team[a], the ASDEX Upgrade Team[b] and JET Contributors[c]

[1] Oak Ridge National Laboratory, Oak Ridge, TN 37831-6305, United States of America
[2] Laboratorio Nacional de Fusión, CIEMAT, Madrid, Spain
[3] MIT Plasma Science and Fusion Center, Cambridge, MA 02139, United States of America
[4] UKAEA, Culham Campus, Abingdon OX14 3DB, United Kingdom of Great Britain and Northern Ireland
[5] Max-Planck-Institut für Plasmaphysik, D-85748 Garching, Germany
[6] Physics Department, Technical University of Munich, TUM School of Natural Sciences, 85748 Garching, Germany
[7] Bernardo Wood Solutions, Estrada de Santo Antonio, n.40, 9360-503 ponta do sol, Madeira, Portugal
[8] Department of Physics, University of Milano-Bicocca, Milano, Italy
[9] National Centre for Nuclear Research, Andrzeja Sołtana 7, 05-400 Otwock, Poland
[10] Commonwealth Fusion Systems, Devens, MA, United States of America

E-mail: delabieeg@ornl.gov

Received 5 September 2025, revised 12 January 2026
Accepted for publication 19 January 2026
Published 2 February 2026

Abstract

The empirical scaling for the H-mode power threshold in tokamaks has been revisited using a database with threshold data from machines with a metallic first wall as part of International Tokamak Physics Activity (ITPA) task TC-26. The database contains discharges from ASDEX Upgrade (AUG) (W), JET (Be/W) and Alcator C-Mod (Mo). This was motivated by reports that in like-for-like discharges the power threshold was reduced by approximately 30% after the change from carbon based to metallic first wall materials on AUG (Ryter *et al* 2013 *Nucl. Fusion* **53** 113003) and JET (Maggi *et al* 2014 *Nucl. Fusion* **54** 023007). The database contains L–H transition data for all hydrogen isotopes and mixtures, including T and DT from the recent JET campaigns. Compared to the ITPA 2008 scaling (Martin *et al* 2008 *J. Phys.: Conf. Ser.* **123** 012033), the metal wall scaling has a smaller magnetic field exponent but a larger density

[a] See Joffrin *et al* 2024 (https://doi.org/10.1088/1741-4326/ad2be4) for the EUROfusion Tokamak Exploitation Team.
[b] See Zohm *et al* 2024 (https://doi.org/10.1088/1741-4326/ad249d) for the ASDEX Upgrade Team.
[c] See Maggi *et al* 2024 (https://doi.org/10.1088/1741-4326/ad3e16) for JET Contributors.
[*] Author to whom any correspondence should be addressed.

exponent. We present an additional parameter to capture the strong dependence of the L–H power threshold (approx. factor 2) on the magnetic configuration in the divertor on JET. The scaling recovers the approximate inverse isotope mass scaling of the threshold power. Alternative scalings involving the plasma current and poloidal magnetic field are explored. Despite the reduction in threshold observed earlier, the scalings based on the metal wall database do not necessarily extrapolate to a lower threshold for ITER compared to the ITPA 2008 scaling, especially at high density. The divertor configuration effect induces the largest uncertainty in the extrapolation.

Supplementary material for this article is available online

Keywords: L–H transition, H-mode power threshold, ITPA scaling

(Some figures may appear in colour only in the online journal)

1. Introduction and motivation

Both ITER as well as future tokamak reactor concepts rely on accessing H-mode energy confinement times to achieve their design goals. The expected heating power that is required to access and stay in H-mode plays an important role in the planning of the ITER operational phases [1] and the heating power that needs to be installed on future reactor grade devices such as EU-DEMO [2]. To enable extrapolation from current experiments, multi-machine databases containing the L–H threshold power along with global plasma and machine parameters have been compiled as part of a long-standing activity within the International Tokamak Physics Activity (ITPA). A recent overview of activities related to L–H transition studies within the ITPA groups is given in [3]. One of the most extensive and widely used L–H threshold scalings is the 2008 ITPA scaling (equation (2) in [4]), which is based on a subset of the International Global Threshold DataBase (IGDBTH) [5–9]. The scaling is reproduced below (equation (1)). $P_{\mathrm{L-H}}$ is the threshold power in MW, $\overline{n_{\mathrm{e}}}$ is the line averaged density in 10^{20} m^{-3}, B_{t} is the vacuum toroidal magnetic field on axis in T and S is the surface area of the last closed flux surface in m^2

$$P_{\mathrm{L-H}}^{2008} = 0.0488 e^{\pm 0.057} \overline{n_{\mathrm{e}}}^{0.717 \pm 0.035} B_{\mathrm{t}}^{0.803 \pm 0.032} S^{0.941 \pm 0.019}. \quad (1)$$

The dataset used for the 2008 ITPA scaling is dominated by machines that have carbon based plasma facing components, unlike ITER which will have a tungsten first wall. The changeover of the first wall materials on ASDEX Upgrade (AUG) from carbon to tungsten and on JET from carbon to beryllium in the main chamber and tungsten in the divertor highlighted a reduction of the threshold power in like-for-like discharges. The threshold decreased by about 25% in AUG in the standard H-mode pulse run at the beginning of each experimental day [10] and the threshold on JET decreased by about 30% at high density in a repeat of identical discharges carried out earlier in the carbon wall environment with the same MkII-HD divertor geometry [11].

The physics reasons for such a change are still debated. Subtracting the bulk radiation from the total heating power on JET yields an even larger reduction in the power crossing the separatrix at the transition between the C-wall and ITER-like wall (ILW) pulses [11]. The observation of lower edge electron temperatures at the transition in both AUG [10] and JET [11], proportional to the lower heating power with the metallic wall, is a further indication that the changes are not due to accounting errors of the power fluxes at the transition and therefore the explanation needs to be sought in the local changes in the edge where the transport barrier forms. Several mechanisms have been proposed based on the hypothesis that the $E \times B$ flow shear is responsible for the turbulence suppression [12]. Recent studies of the radial electric field in the edge of AUG [13] and JET [14] L-mode plasmas show that the radial electric field exhibits a complex structure with both the main ion diamagnetic pressure as well as the flow terms playing a role. A mechanism based on the contribution of the main ion diamagnetic pressure to the radial electric field is proposed in [15]. A higher edge density is observed in W-wall discharges in AUG [15] compared ot C-wall discharges. The higher density gradient contributes to the depth of the E_{r} well according to the radial force balance equation, matching similar values as for the C-wall but at lower power with the W-wall. The cause for the change in density is attributed to the higher reflection coefficient of neutral particles recycling from tungsten surfaces and is reproduced in EMC3-EIRENE simulations [16]. A comparison between edge density profiles before and after the installation of the Be/W on JET did not show such a difference in the density gradient [17]. Another empirical difference between AUG and JET is the observation that the threshold on JET-ILW could be increased back to similar values as on JET-C by the injection of nitrogen [18, 19], which has not been observed on AUG [10]. A mechanism that has been proposed to explain the change in power threshold in the high density branch is that an increase in Z_{eff} increases the resistive turbulence drive [20], and thus more power is needed to reach a sufficiently high E_{r} shearing rate. Another mechanism for low-Z impurities to influence the threshold is via localised electron cooling in the scrape off layer (SOL) and divertor. This could reduce

the strength of the sheath voltage at the strike points, and thus the strength of the positive E_r in the near SOL [21].

In the current paper we are not attempting to identify the physics mechanisms responsible for the reduction in threshold, but we are investigating if the changes in the L–H threshold power that have been reported in like-for-like discharges in AUG and JET due to the presence of metallic walls also change the global scaling of the threshold power by constructing a more extensive database using data from devices with metallic plasma facing components: AUG (W), JET (Be/W) and Alcator C-Mod (Mo). This paper is organised as follows: section 2 describes the data selection and references the experiments contributing to the database. Section 3 describes the fitting methodology with the results shown in section 4. Section 5 discusses the density for H-mode access at minimal power. Section 6 discusses the implications for ITER and SPARC with an outlook and discussion in section 7. Section 8 summarizes the conclusions.

2. Data selection

The 2008 ITPA scaling [4] is based on a selection of data that is considered most ITER-relevant: conventional aspect ratio, diverted single null with the ion $B \times \nabla B$-drift towards the divertor (favourable) and a plasma density above the density at which the minimum in the threshold occurs ($n_{e,min}$). Those selection criteria also apply to the data used here with the addition that we have broadened the selection criteria to include hydrogen and tritium discharges as well as mixtures, while continuing to exclude helium discharges. Discharges with impurity seeding or exhibiting signs of impurity accumulation such as high core radiation or hollow temperature profiles have been excluded. The datatypes collected have the same definitions as in prior ITPA confinement databases. Any reference to the L–H threshold power in this paper is referring to the loss power (equation (2)), which is the total of the ohmic and absorbed heating power corrected for the increase in stored energy in order to obtain the power flowing through the separatrix

$$P_{loss} = P_{\Omega} + P_{heat}^{abs} - \frac{dW}{dt}. \quad (2)$$

The bulk radiation has not been subtracted from the loss power for the recommended scalings presented here. The rationale for this is explained in section 4 along an analysis of the core radiation on the scaling: distinguishing core radiation from radiation outside the last closed flux surface can be prone to diagnostic artefacts which are machine specific, and the main purpose of the scaling is to provide the required heating power that needs to be installed based on engineering parameters or variables that can be controlled.

For discharges that exhibit dithering transition, the consensus is to choose the transition time at the final transition into H-mode. The database does not distinguish between the type of H-mode that is obtained, nor the confinement properties above threshold.

Only transitions in the so-called high density branch (densities above $n_{e,min}$) are taken into account for the scaling, although the database also contains low density transitions. The selection criteria chosen to distinguish between low and high density branches are shown in table 1 and discussed in section 5. The value of $n_{e,min}$ depends on the combination of field and current, isotope mass and, for JET, the magnetic configuration in the divertor. The values of $n_{e,min}$ have been empirically established when density scans at otherwise fixed variables are available in the database. Table 2 gives an overview of the number of transitions per tokamak and the parameter ranges for each device. A total of 481 transitions have been selected for the scaling, compared to 1024 datapoints being used for the ITPA 2008 scaling [4].

The TC-26 database is available as an auxiliary file to this paper.

2.1. ASDEX Upgrade (AUG)

The initial description of the experiments showing the reduction in P_{L-H} following the change from the carbon to the tungsten wall is presented in [10]. An overview of more recent L–H transition experiments on AUG is given in [22]. Figure 1 shows the high density branch threshold data overplotted on the 2008 ITPA dataset versus the 2008 scaling, clearly showing all the metal wall deuterium threshold power data to be below the scaling. The experiments in hydrogen are described in [23, 24] and are all above the scaling, approximately a factor of 2 above the deuterium data. $n_{e,min}$ is slightly higher in hydrogen [23] and also increases with plasma current [25]. The dataset mainly contains NBI and ECRH heated discharges, but also some with ICRH heating. Most of the data are at $B_t = 2.3-2.4$ T, but with some variation between 1.6 T and 3 T [26]. When normalising the data over the 2008 scaling and plotting against the variable in that scaling, there is no clear trend with density but the new data seems to show a slightly weaker B_t dependence, see figure 1(*b*). Dedicated B_t scans in AUG, at approximately fixed density, have shown an increase of the threshold with B_t (e.g. [26]). All pulses have the strike points on the vertical divertor targets as shown in figure 2(*a*). Experiments investigating the effect of the magnetic configuration in the lower divertor of AUG, as used in this database, have so far not shown a clear effect on the threshold power.

2.2. Alcator C-Mod (C-Mod)

The Alcator C-Mod data takes a distinct place in the database, operating at higher magnetic field and density than AUG and JET, albeit with a smaller minor radius. A description of L–H transition experiments for which data has been contributed to the database can be found in [27] for the 5.3 T data and in [28] for the data at 7.7 T. The 5.3 T discharges are all heated with ICRH hydrogen minority heating, whereas the 7.7 T discharges are using a ^{3}He minority heating scheme. Alcator

Table 1. Selection criteria used to select high density branch transitions. If the density is indicated to be below a certain value then the low density branch was not experimentally accessed and the minimum could be below the stated value.

Tokamak	isotope	B_t [T]	I_p[MA]	divertor config.	$n_{e,min}[10^{19}$ m$^{-3}]$	$P_{n_{e,min}}$ [MW]
AUG	H	2.3–2.5	0.8–1.12	STANDARD	4.5	2.5
	D	2.35	0.6	STANDARD	2.5	0.8
	D	1.7–2.35	0.8	STANDARD	3.0	1.0
	D	2.35	1.0	STANDARD	3.5	1.3
C-Mod	D	5.3–7.7	0.65–1.4	VERTPLT	14.0	1.5
JET-ILW	D	1.3	1.25–1.35	CORNER	<1.7	<2.0
	H	1.8	1.7	HT	3.1	5.0
	D	1.8	1.7	HT	2.2	1.5
	DT/T	1.8	1.7	HT	<2.0	<1.0
	H	1.8	1.7	CORNER	<1.7	<6.5
	D	1.8	1.7	CORNER	<2.0	<3
	D	2.4	1.5	HT	<2.2	<1.5
	D	2.4	2.0	HT (V5L)	2.7	1.75
	D	2.4	2.0	HT	2.85	3.0
	T	2.4	2.0	HT	2.2	1.25
	D	2.4	2.0	VT/CORNER	2.0	3.0
	D	3.0	2.5–2.75	HT	3.2	4.5
	DT	3.0	2.5–2.75	HT	3.1	3.0
	T	3.0	2.5–2.75	HT	2.7	2.0
	D	3.0	2.5	VT	2.3	5.0
	D	2.8-3.7	2.5–4.0	CORNER	2.5 (unclear)	6.5 (unclear)

Table 2. Overview of the number of transitions in the database and parameters range per tokamak.

Tokamak	# transitions	# transitions $n_e > n_{e,min}$	B_t [T]	I_p [MA]	$\overline{n_e}$ [10^{19} m^{-3}]	S [m^2]
AUG	252	162	1.69–2.98	0.60–1.01	2.58–6.79	43.8
C-Mod	77	58	5.27–7.67	0.63–1.78	14.0–28.7	7.37
JET-ILW	360	261	1.29–3.68	1.23–3.94	1.41–6.43	139

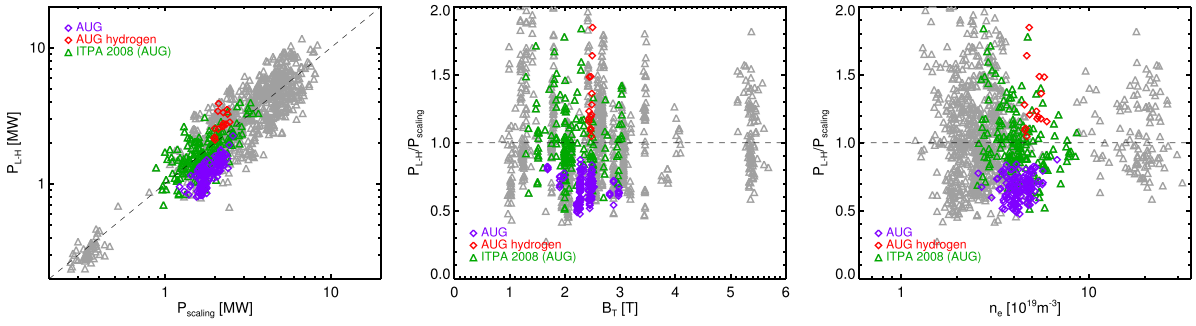

(a) P_{L-H} vs. P^{2008}_{L-H}. (b) $\mathrm{P}_{L-H}/\mathrm{P}^{2008}_{L-H}$ vs. B_t. (c) $\mathrm{P}_{L-H}/\mathrm{P}^{2008}_{L-H}$ vs. $\overline{n_e}$.

Figure 1. Overview of AUG $P_{\mathrm{L-H}}$ data (purple: deuterium discharges, red: hydrogen discharges), overplotted on the ITPA 2008 dataset (green: AUG only, grey: other tokamaks).

C-Mod has always operated with molybdenum plasma facing components, and, thus, metal wall threshold data had been contributed already to the ITPA database before this study. However, here we have only used post-2008 data because of improved accounting for the ICRH heating efficiency and core radiated power fraction. Figure 3 shows $P_{\mathrm{L-H}}$ normalized over the 2008 ITPA scaling versus $\overline{n_e}$ and B_t. The trend with magnetic field appears weaker than the scaling [28]. In fact, no clear B_t scaling can be discerned in the C-Mod P_{loss} data. However, the analysis of a distinct set of L–H transition on C-Mod [29] showed that relatively low P_{loss} at the highest C-Mod fields was accompanied by an increased edge ion heat flux $Q_{\mathrm{i,edge}}$, due primarily to the higher direct ion heating realized with ICRH with D(^{3}He) at ≈8 T. The combined analysis of C-Mod and AUG $Q_{\mathrm{i,edge}}$ indicated that $Q_{\mathrm{i,edge}}$ increases with B_t. It is unknown whether this trend persists in the TC-26 database,

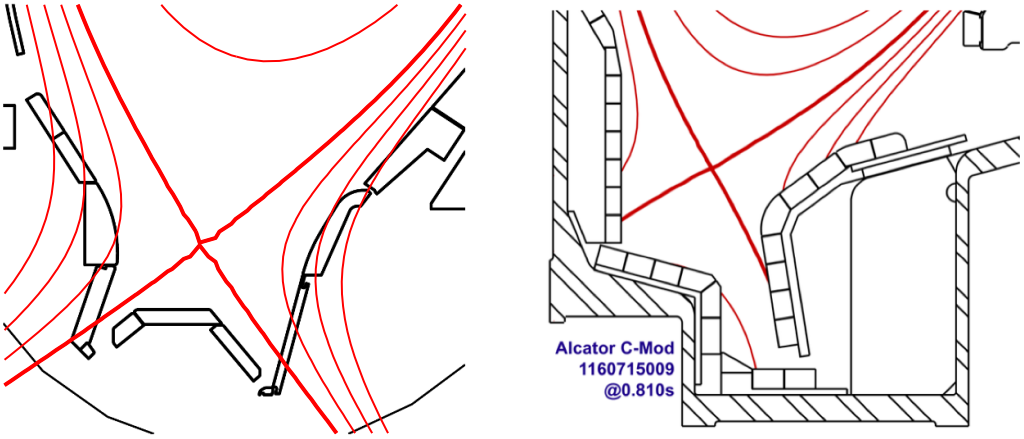

(a) Magnetic configuration for an AUG discharge in the database (labelled STANDARD) .

(b) Magnetic configuration for one of the 8T discharges in the database (labelled VERTPLT).

Figure 2. Magnetic configuration in the divertor for the AUG and C-Mod discharges in the TC-26 database.

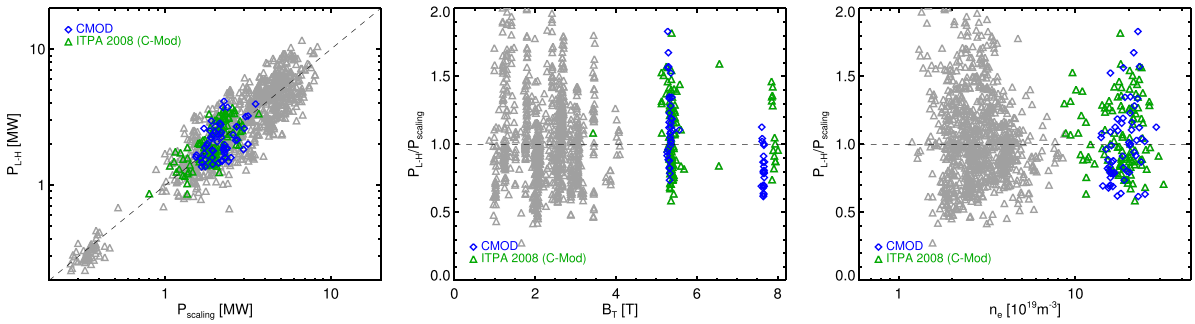

(a) P_{L-H} vs. P^{2008}_{L-H}. (b) $\mathrm{P}_{L-H}/\mathrm{P}^{2008}_{L-H}$ vs. B_t. (c) $\mathrm{P}_{L-H}/\mathrm{P}^{2008}_{L-H}$ vs. $\overline{n_e}$.

Figure 3. Overview of Alcator C-Mod $P_{\mathrm{L-H}}$ data (blue), overplotted on the ITPA 2008 dataset (green: C-Mod only, grey: other tokamaks).

as calculation of $Q_{\mathrm{i,edge}}$ is not feasible over the entire database. Therefore we exercise caution about deducing a weak power threshold scaling on B_{t} from the C-Mod data alone. All C-Mod data in the database are in a configuration with the outer strike point on the vertical divertor plate as shown in figure 2(*b*) [27, 28]. C-Mod discharges with reduced power threshold, having extended outer leg length and strike on a horizontal plate [30], could be added as part of future extensions to the database.

2.3. Joint European Torus with the ITER-like wall (JET-ILW)

The largest contribution to the TC-26 database comes from JET with 360 entries. The initial experiments with the Be/W wall [11] were aimed at repeating reference discharges carried out with the carbon wall with the same MkII-HD divertor geometry for 1-to-1 comparisons and were focused at three values of magnetic field: 1.8 T, 2.4 T and 3.0 T at nearly constant $q_{95} = 3.3-3.7$. A more recent overview of L–H transition experiments on JET is presented in [31, 32]. The JET dataset contains transitions for a range of magnetic configurations in the divertor, which was known from C-wall experiments [33] to have an effect on the threshold. The divertor configuration effect was found to change the threshold by as much as a factor 2 between configurations on JET-ILW, as well as the value of $n_{\mathrm{e,min}}$ [11, 19, 34]. Figure 4 shows the three main groups of configurations in the database: the horizontal target (HT) configuration has the outer strike point on the horizontal tile 5 and the inner strike point on the vertical target (figure 4(*a*)), the corner configuration with both strike points close to the pumping ducts in the corners (figure 4(*b*)), and the vertical target (VT) configuration with both strike points on the vertical targets (figure 4(*c*)). The VT and CORNER configuration have a similar, higher, threshold and a lower $n_{\mathrm{e,min}}$ and are grouped together within this study. Within the HT discharges there is a continuous decrease in threshold and $n_{\mathrm{e,min}}$ as the outer strike point moves to lower major radius while the inner strike point is kept on the vertical target. One of these configurations, labelled V5L, is singled out in table 1 because we have used a slightly lower $n_{\mathrm{e,min}}$ for distinguishing high from low density branch transitions for this configuration. This configuration is shown as the dashed configuration in figure 4(*a*) and is considered part of the HT group in this work albeit with a slightly lower $P_{\mathrm{L-H}}$ than HT configurations that have the outer

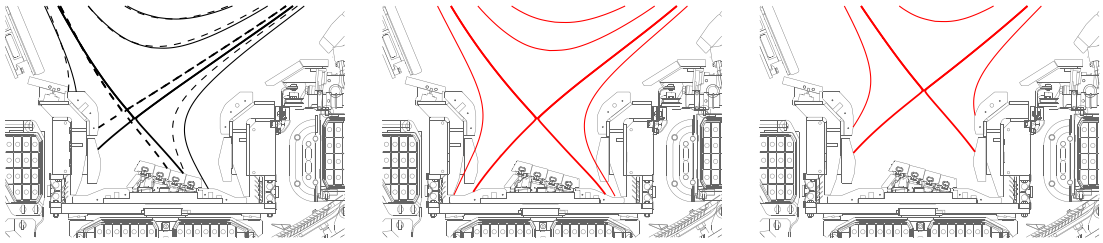

(a) Horizontal target configurations (HT). The dashed configuration is called V5L in table 1.

(b) Corner configuration (CORNER).

(c) Vertical target configuration (VT).

Figure 4. Magnetic configuration in the divertor on JET. The VT and CORNER configurations are grouped together in the scaling.

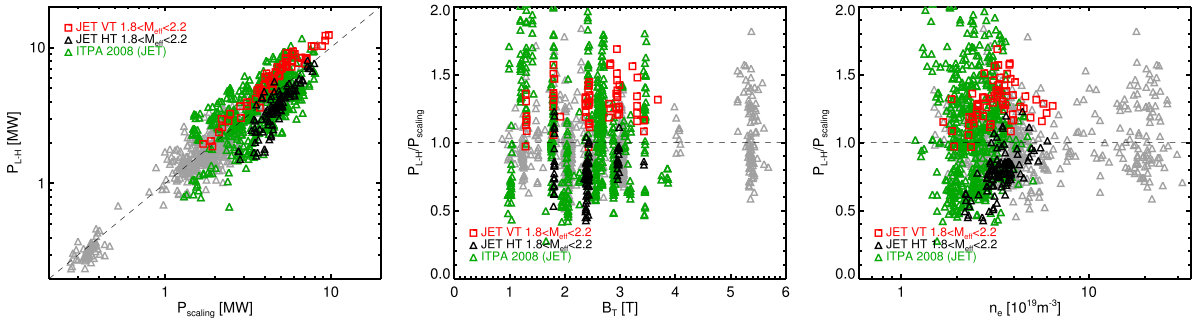

(a) P_{L-H} vs. P^{2008}_{L-H}.

(b) $\mathrm{P}_{L-H}/\mathrm{P}^{2008}_{L-H}$ vs. B_t.

(c) $\mathrm{P}_{L-H}/\mathrm{P}^{2008}_{L-H}$ vs. $\overline{n_e}$.

Figure 5. Overview of JET $P_{\mathrm{L-H}}$ data for M_{eff} close to 2, overplotted on the ITPA 2008 dataset (green: JET only, grey: other tokamaks). Red squares are JET-ILW discharges in vertical and corner configuration data and black triangles are JET-ILW discharges with the outer strike point on the horizontal target.

strike point at larger major radius. Figure 5 shows the JET-ILW data with M_{eff} close to 2 overplotted on the 2008 ITPA database. This shows that the HT and VT discharges form two distinct groups. There is a reduction in threshold with regard to the 2008 ITPA scaling for HT configuration discharges, but most VT configuration discharges have a threshold above the 2008 scaling. Figure 5(*c*) shows a tendency for a stronger increase of the threshold power with density compared to the 2008 ITPA scaling, especially for the HT configuration. The origin of the divertor configuration effect is not yet understood. A proposed mechanism is that a change in recycling pattern affects the electron temperature at the target which causes the sheath voltage and the radial electric field (E_{r}) in the near-SOL to change and therefore the $E \times B$ shear across the separatrix [21, 35]. A more positive E_{r} in the SOL increases the $E \times B$ flow in the SOL driving more heat towards the outer target, at the expense of the inner target, increasing the sheath voltage further. On JET, a correlation is found in the HT configuration between the sudden increase of the outer target electron temperature, the detachment of the inner strike point and the L–H transition [35]. The perpendicular flow measured by Doppler backscattering corroborates the appearance of a peak in the near-SOL E_{r} before the transition in HT configuration but does not find a critical E_{r} shear between the configurations that would be required to reach the L–H transition [14].

The database contains data in hydrogen, deuterium, tritium and all mixtures thereof [31, 32, 36–39]. The threshold for both H–D [36] and H–T [39] mixtures has been observed to not change linearly with concentration, the detailed reasons of this could be specific to the experiments, such as the ICRH heating schemes and peculiar transport effects of isotope mixtures, and are difficult to capture with a scaling. The value of $n_{\mathrm{e,min}}$ is affected by divertor configuration, isotope mass [32], I_{p} and potentially B_{t}. Table 1 shows an overview of the selection criteria used to distinguish between low and high density branch transitions. Apart from a few Ohmic transitions in tritium, the majority of the transition data comes from power ramps at constant density, typically at 1 MW s^{-1}, using either ICRH or NBI heating. An exception are the pulses that appear with the highest thresholds in figures 5 and 6 with plasma current up to 4 MA. These come from the program developing the so-called baseline scenario towards high current for the D-T experiments [40]. They have faster and less smooth ramp rates, suffering from more regular neutral beam breakdowns. We are using the stored energy from the diamagnetic loops to calculate $\mathrm{d}W/\mathrm{d}t$, which is typically an overestimate of the stored energy in L-mode [41]. On average $|\mathrm{d}W/\mathrm{d}t|/P_{\mathrm{L-H}} = 6\%$, so the uncertainty induced by the ramp rate is small, but for the 5 pulses with highest threshold in deuterium this is 10%, therefore leading to a potential overcorrection.

3. Methods

Similar to [4], the loss power is fitted using a power law of the form:

$$P_{\mathrm{L-H}} = \alpha\, B_{\mathrm{t}}^{\beta}\, I_{\mathrm{p}}^{\gamma}\, B_{\mathrm{pol}}^{\delta}\, \overline{n_{\mathrm{e}}}^{\epsilon}\, 2/M_{\mathrm{eff}}^{\zeta}\, D\, S^{\eta}. \tag{3}$$

The units are MW, T, MA, 10^{20} m^{-3} and m^2. This reverts to the same power law as the 2008 ITPA scaling when $\gamma = \delta = 0$ and $D = 1$. The additional fit variables account for isotope and divertor configuration effects. The effective mass in the scaling is the main ion mass in atomic mass units weighted over the isotope fractions: $M_{\mathrm{eff}} = f_{\mathrm{H}} m_{\mathrm{H}} + f_{\mathrm{D}} m_{\mathrm{D}} + f_{\mathrm{T}} m_{\mathrm{T}}$. S is the surface area of the last closed flux surface as obtained from a magnetic reconstruction. $\overline{n_{\mathrm{e}}}$ is the line averaged electron density. The toroidal magnetic field tends to be correlated with the plasma current within the data obtained from a single device, as most devices operate within a relatively narrow q_{95} range. Table 3 lists the correlation coefficients between density, magnetic field and plasma current for the data from each device. Therefore we have also alternatively fitted the data using I_{p} as engineering fit parameter and the averaged B_{pol} at the separatrix as the underlying physical parameter. B_{pol} has been calculated as: $B_{\mathrm{pol}} = 2\pi\mu_0 I_{\mathrm{p}}\mathrm{R/S}$. The fit parameter D in equation (3) accounts for the divertor configuration effect observed in the JET data. The parameter is fixed to 1 in the fit for the JET HT configuration as well as for the AUG and C-Mod data, but left as a free parameter for the JET VT and CORNER configurations. The choice to group the JET HT, the AUG and C-Mod data together is retro-actively verified in figure 10 which shows the data normalised to the fit apart from a single fit parameter. Normalising over the surface area is sufficient to align the JET HT with the AUG data. The C-mod data occupies a different B_{t} and $\overline{n_{\mathrm{e}}}$ space, but aligns well with the trend of the lower threshold group. The decision to consider the JET VT data anomalously high and to keep C-Mod in the same group as AUG also helps to reduce inter-machine bias. Because there are only 3 devices in the current dataset, the exponent of the surface area, η, has been put to 1 ($\eta = 1$ in equation (3)). This is also motivated by the $S^{0.94}$ scaling in the 2008 ITPA dataset which had a larger range of devices and by the physics intuition that the heat flux through the separatrix (for which P/S is a proxy) is the critical parameter for the transition.

The procedure used to derive the 2008 ITPA scaling in [4] is an unweighted logarithmic χ^2 minimization. The use of the logarithm slightly reduces the bias towards datapoints with a higher threshold compared to an unweighted linear χ^2 optimization. For this work we have decided to use a χ^2 minimization with weights that are proportional to $P_{\mathrm{L-H}}$ (equation (4)).

$$\chi^2 = \sum \left(\frac{P_{\mathrm{L-H}} - P_{\mathrm{scal}}}{0.15\, P_{\mathrm{L-H}}} \right)^2. \tag{4}$$

This results in the relative deviation with regard to the scaling of each datapoint to have the same relative contribution to χ^2. The effect of the different minimization has been evaluated by applying the linear weighted χ^2 fit to the ITPA 2008 database. The results are close to the logarithmic fit, albeit for a small reduction of the surface area exponent that would lower the threshold prediction for ITER (see table 4).

As uncertainty on each datapoint, a 15% errorbar on the threshold power has been chosen. This is rather arbitrary, but does not affect the optimised fit parameters. It only rescales the uncertainties on the fit parameters which are calculated from the diagonal elements of the covariance matrix. It is important to note that the uncertainties are only meaningful if the power law fitted to the data would be an accurate representation for the dataset. For extrapolation using the scaling, uncertainties associated with the divertor configuration effect and choice of fit parameters are more significant than the statistical uncertainties from the fit. The root of the mean of the normalised squared errors (RMSEs) is taken as a measure for the quality of the fit.

4. The TC-26 database scalings

4.1. Scalings for $P_{\mathrm{L-H}}$

To identify trends common to the threshold power in the three devices, we first fit the data from each machine individually. Table 4 shows an overview of the resulting fit parameters of all the fits that have been carried out. An observation common to the three devices is that when using the same fit variables as in the 2008 ITPA scaling ($\overline{n_{\mathrm{e}}}$, B_{t}) but with the addition of M_{eff} and D and keeping S fixed, there is a tendency for a lower B_{t} exponent and a higher $\overline{n_{\mathrm{e}}}$ exponent. This is also reflected in the fit to the entire TC-26 database, shown in equation (5) and labelled TC-26 (B_{t}) in table 4.

$$\begin{aligned} P_{\mathrm{L-H}}^{\mathrm{TC-26}(B_{\mathrm{t}})}/S = {} & 0.0441 \pm 0.0025\, B_{\mathrm{t}}^{0.580\pm0.039}\, \overline{n_{\mathrm{e}}}^{1.08\pm0.03} \\ & \times 2/M_{\mathrm{eff}}^{0.975\pm0.032}\, D \\ & \text{with D} = 1 \text{ for a HT-like divertor configuration} \\ & \text{and D} = 1.93 \text{ for a VT-like divertor configuration.} \end{aligned} \tag{5}$$

The factor D that accounts for the divertor configuration effect on JET gives a factor 1.93 difference between the configurations when fitting the entire database and a factor 1.73 when fitting only the JET data. The fit to the effective mass, $M_{\mathrm{eff}}^{-0.975}$, is very close to the $1/M_{\mathrm{eff}}$ scaling reported following the DTE1 experiments on JET [42] and in agreement with the increase in threshold shown on many devices when changing the plasma composition from D to H. Figure 6(a) show the entire threshold database versus the TC-26 (B_{t}) scaling, showing good alignment for the three devices.

It is interesting to note that the sum of the density and B_{t} exponents remains close to the 2008 scaling. This requires us to investigate to which degree these variables are correlated within the database. Since most machines operate within a narrow range of q_{95}, this can induce a correlation between B_{t} and I_{p}. Because the plasma current also changes the value of $n_{\mathrm{e,min}}$, this reinforces the correlation between density and

Table 3. Correlation coefficients between variables in the database, per device.

Tokamak	cor(B_t, $\overline{n_e}$)	cor(B_t,I_p)	cor($\overline{n_e}$,I_p)
AUG	0.028	0.292	0.512
C-Mod	0.009	0.371	0.608
JET-ILW	0.522	0.832	0.586

plasma current which is already naturally present in L-mode discharges. Table 3 shows the Pearson linear correlation coefficient between B_t, $\overline{n_e}$ and I_p. This indicates that the density and field are very weakly correlated within the AUG and C-Mod datasets but moderately correlated on JET. The magnetic field and plasma current are strongly correlated within the JET dataset and moderately on AUG and C-Mod. This leads to the question to which degree a plasma current based scaling would fit the data. The investigation of a plasma current based fit is also motivated by the observation that P_{L-H} normalized to the TC-26(B_t) fit shows a positive trend with plasma current for AUG, C-MOD and the HT configuration on JET as shown in figure 7. For the VT configuration on JET, the trend is negative, strongly influenced by the potentially underestimated threshold of the highest I_p discharges from the baseline development program. A fit using both B_t and I_p, in addition to the fit parameters used in the TC-26 (B_t) fit, is labelled TC-26 (B_t,I_p) in table 4. The fit labelled TC-26 (B_{pol}) uses the poloidally averaged B_{pol} at the separatrix as a fit parameter instead of B_t. B_{pol} at the separatrix is a physically more meaningful quantity for the effect of the plasma current on the plasma edge. The fit using both B_t and I_p finds a weak scaling with plasma current $I_p^{0.235}$ at the expense of a reduced B_t exponent. The additional fit variable reduces the RMSE of the fit, as expected. Remarkably, the fit using only B_{pol} has a lower RMSE than the fit using both B_t and I_p. On a single device, I_p and B_{pol} would be nearly interchangeable fit variables. The improvement in RMSE compared to the scaling using both B_t and I_p must therefore come from the approximate $1/a$ dependence intrinsic to the definition of B_{pol}. To see if this is a side effect of fixing the surface area exponent to 1, a fit (labelled TC-26 (B_t,S) in table 4) was made leaving this exponent free, yielding $S^{1.14}$. The RMSE of this fit is still higher than the B_{pol} based scaling. The effect of B_{pol} on the threshold, as an alternative to the more traditional B_t based scaling, would be a worthwhile subject for more investigation, both at high density and close to $n_{e,min}$.

4.2. Influence of core radiation

Previous studies using subsets of the data in this database have shown better alignment, in particular between NBI and ICRH heated discharges [32], when subtracting the core radiation from the loss power. In order to investigate the effect of core radiation over the entire database, we have used a definition of the core radiation for the three devices that is as unified as possible. For C-Mod, reliable core radiative power data is only available for the 5.3 T dataset and is based on the inversion of foil bolometer signals looking horizontally near the midplane [43]. The inverted emissivity is then integrated to the separatrix. For AUG and JET we have used the integrated emissivity from a tomographic reconstruction of the bolometry signals (see [44] for AUG) up to $r/a = 0.95$. The reason for this choice is the limited spatial resolution of the bolometry diagnostics near the LCFS and the strong radiation in the divertor region near the X-point, which creates ambiguity in the distinction between core and divertor radiation. The latter is also excluded from the C-Mod data due to only midplane lines of sight being used in the analysis. The radiation normalized over the threshold power (f_{rad}) is shown in figure 8 for the three devices as function of density. Within the data of each device, there is no trend in f_{rad} with regard to any of the variables used for the scaling, but there is a large increase in the scatter when subtracting the radiation from the threshold power. ICRH discharges on JET tend to have higher f_{rad} than NBI heated discharges (see figure 8). The radiation fraction averaged over all devices is 20%. When subtracting the radiation from P_{L-H} we can derive a scaling for P_{sep} using the subset for which reliable P_{rad} data is available, see equation (6) (not recommended for extrapolation).

$$\begin{aligned} P_{sep}^{TC-26(B_t,P_{sep})}/S = 0.030 \pm 0.002\ & B_t^{0.73\pm0.05}\ \overline{n_e}^{1.07\pm0.03} \\ & \times 2/M_{eff}^{0.97\pm0.03}\ D \\ \text{with D} = 1 &\text{ for a HT-like divertor configuration} \\ \text{and D} = 2.17 &\text{ for a VT-like divertor configuration} \\ \text{RMSE} = 0.280.& \end{aligned} \tag{6}$$

Apart from an obvious reduction in the pre-factor, there is a large increase in the RMSE of the fit to 28% due to the scatter caused by the core radiation measurements. There is a modest increase in the magnetic field exponent and in the parameter accounting for the divertor configuration effect. The first is likely an inter-machine bias caused by the C-Mod data exhibiting a slightly lower f_{rad}, within the uncertainty induced by the diagnostic differences between the devices and the different method used to calculate the core radiated power. The second is caused by a bias between ICRH and NBI heated discharges on JET as nearly all ICRH transitions are in the HT configuration. Despite the fact that accounting for the core radiation when studying a dedicated experimental dataset leads to results that are inline with the physics intuition, the combination of high scatter (high RMSE) and inter-machine diagnostic bias lead to the

Table 4. Overview of fit parameters for various fits to the 2008 and TC-26 ITPA databases. The TC-26(B_t) scaling is indicated in bold.

Dataset	η (S)	α (pre-factor)	β (B_t)	γ (I_p)	δ (B_{pol})	ϵ ($\overline{n_e}$)	ζ (M_{eff})	D	RMSE
ITPA 2008 (log-linear) [4]	0.941 ± 0.019	$0.0488\ e^{\pm 0.057}$	0.803 ± 0.032	—	—	0.717 ± 0.035	—	—	0.307
ITPA 2008 (least-quares)	0.885 ± 0.010	0.0500 ± 0.0014	0.851 ± 0.016	—	—	0.689 ± 0.018	—	—	0.274
C-Mod only	1	0.157 ± 0.034	-0.075 ± 0.112	—	—	1.10 ± 0.12	1	1	0.207
AUG only	1	0.0314 ± 0.0042	0.689 ± 0.127	—	—	0.949 ± 0.0904	0.890 ± 0.064	1	0.142
JET-ILW only	1	0.0687 ± 0.0053	0.474 ± 0.051	—	—	1.22 ± 0.043	1.11 ± 0.04	1.73 ± 0.04	0.207
TC-26 (B_t)	**1**	$\mathbf{0.0441 \pm 0.0025}$	$\mathbf{0.580 \pm 0.039}$	**—**	**—**	$\mathbf{1.08 \pm 0.03}$	$\mathbf{0.975 \pm 0.032}$	$\mathbf{1.93 \pm 0.04}$	**0.238**
TC-26 (B_t,S)	1.14 ± 0.02	0.0300 ± 0.0021	0.566 ± 0.039	—	—	1.27 ± 0.03	0.996 ± 0.031	1.81 ± 0.04	0.220
TC-26 (B_t,I_p)	1	0.0585 ± 0.0034	0.390 ± 0.042	0.233 ± 0.019	—	1.22 ± 0.03	1.01 ± 0.03	1.73 ± 0.04	0.201
TC-26 (B_{pol})	1	0.166 ± 0.006	—	—	0.631 ± 0.033	1.07 ± 0.02	1.01 ± 0.03	1.67 ± 0.04	0.189

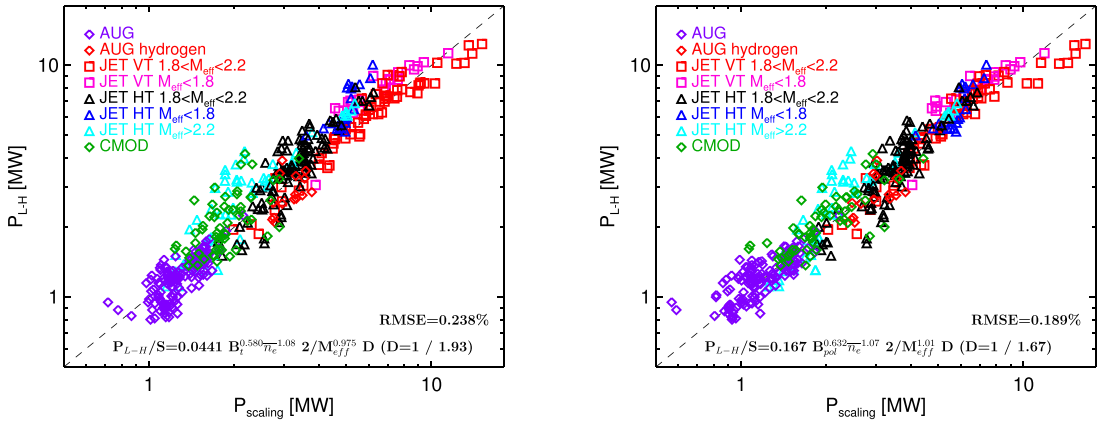

(a) Scaling using B_t as a fit parameter. (b) Scaling using B_{pol} as a fit parameter.

Figure 6. The entire TC-26 $P_{\mathrm{L-H}}$ database plotted versus the TC-26(B_{t}) and TC-26(B_{pol}) threshold scalings. The multiplication factor D is 1 for a HT-like divertor configuration and takes the higher value for a VT-like configuration.

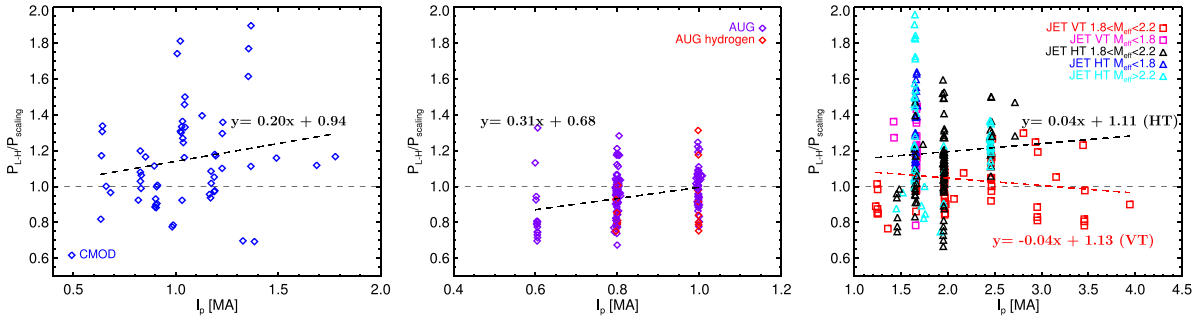

(a) C-Mod (b) AUG (c) JET

Figure 7. $P_{\mathrm{L-H}}$ normalized to the TC-26 (B_{t}) scaling as function of plasma current for each device. The dashed lines indicate trendlines fitted to the data.

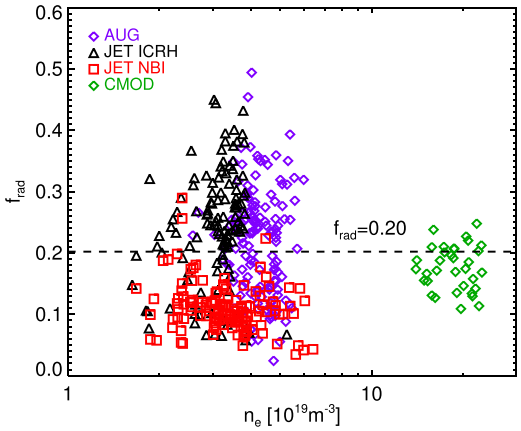

Figure 8. The fraction of core radiation ($f_{\mathrm{rad}} = P_{\mathrm{rad,core}}/P_{\mathrm{L-H}}$) for the three devices as function of line averaged density for all high density branch transitions. There is no trend as function of any of the variables in the scaling law within each individual dataset. Average radiation fraction is 20%.

P_{sep} scaling not being recommended for extrapolation at the present time. Diagnostic differences between devices is also the reason the core radiation is not subtracted in earlier ITPA scalings.

5. Density for H-mode access at minimal power

The density at which the threshold power is minimal is crucial for determining the minimal heating power required to

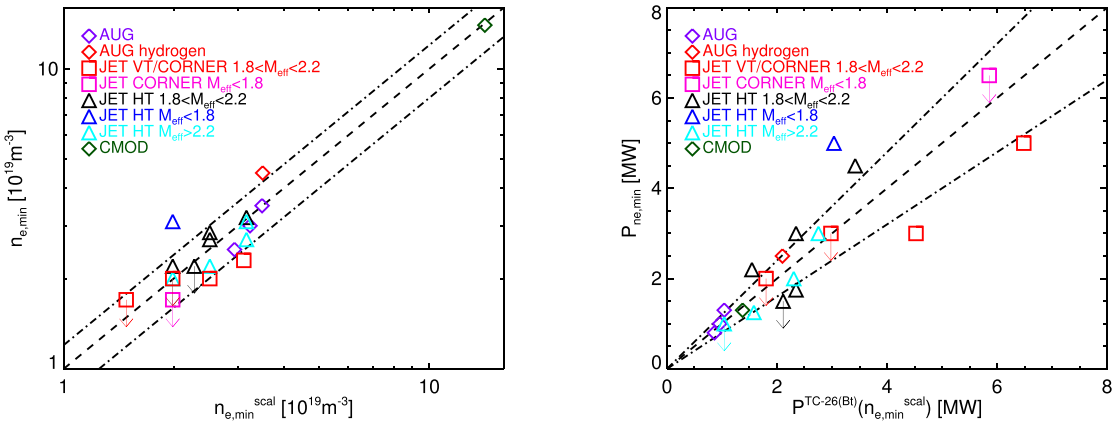

(a) Observed $n_{e,min}$ vs. predicted $n_{e,min}$ according to the scaling from [25]

(b) Observed threshold power vs. predicted power by evaluating the TC-26(B_t) scaling at the predicted value of $n_{e,min}$.

Figure 9. Comparison between the predicted and observed density and power at minimal threshold for the various datasets from table 1. The upper and lower dashed lines indicate a 20% deviation. The arrows indicate that the datapoint is an upper estimate.

access H-mode. Therefore, we compare the experimental values from table 1, which have been obtained by investigating density scans within the database, with the semi-empirical scaling proposed in equation (3) of [25]. The scaling is derived on the premise of the electron–ion heat equilibration time falling below a certain value compared to the energy confinement time and is mainly applicable to electron heated discharges. Although the scaling is derived for deuterium, one can retain the ion mass in the scalings for the L–H threshold, the confinement time and the electron–ion equipartition. As noted in [23, 45], this only yields a very weak ion mass effect, $n_{\mathrm{e,min}} \propto M^{-0.02}$, which is considerably weaker than experimentally reported here. Figure 9(*a*) compares the observed $n_{\mathrm{e,min}}$ with the scaling. The dashed lines indicate a 20% deviation. We note a fair agreement between the scaling and the experimental data despite the scaling not capturing the isotope mass effect and the strong effect of the divertor configuration on $n_{\mathrm{e,min}}$. The hydrogen datasets tend to have $n_{\mathrm{e,min}}$ higher than predicted by the scaling, whereas the tritium datasets tend to fall slightly below the prediction. The JET CORNER and VT datasets have an $n_{\mathrm{e,min}}$ that is most overestimated by the scaling. Figure 9(*b*) shows the observed threshold power ($P_{n_{\mathrm{e,min}}}$) at $n_{\mathrm{e,min}}$ versus the expected threshold power using the TC-26(B_t) scaling and $n_{\mathrm{e,min}}$ derived from the scaling in [25]. This shows how the prediction for the minimal power required to access H-mode performs for a certain device, ion mass and B_t/I_p combination if $n_{\mathrm{e,min}}$ would be unknown but with knowledge of which value to use for the divertor configuration effect in the scaling. This again shows fair agreement. Note that $P_{n_{\mathrm{e,min}}}$ falls below the prediction for the VT and CORNER configuration and $P_{n_{\mathrm{e,min}}}$ is almost equal with the HT configuration. This is because this configuration has lower $n_{\mathrm{e,min}}$, but a higher threshold and both effects tend to compensate each other. This indicates that although the divertor configuration effect is a major unknown for future devices, as far as $P_{n_{\mathrm{e,min}}}$ is concerned, the uncertainty is somewhat mitigated as long as $n_{\mathrm{e,min}}$ is experimentally accessible and within the operational limits of the heating systems.

6. Implications for ITER and SPARC

For extrapolation to ITER, the following machine parameters are assumed: $S = 680$ m^2, $B_t = 5.3$ T, $I_p = 15$ MA, $R = 6.2$ m [46]. Table 5 shows the predicted threshold power at full field and current and for line averaged densities of 0.5 10^{20} m^{-3} and 1.0 10^{20} m^{-3}. The TC-26 (B_t) scaling predicts a slightly reduced threshold for ITER when assuming a favourable divertor configuration ($D = 1$), but a considerably higher threshold if the threshold on ITER would behave more like JET when operating with the strike points on the vertical targets. A detailed assessment of the available heating power during the various phases of the new ITER operational plan [1] compared to both the 2008 ITPA and the TC-26 (B_t) scaling is given in [47]. H-mode access during the first phase of scientific research operation at half field with wave heating only at a Greenwald fraction (f_{GW}) of 0.5 is secure according to the scalings. During DT-1, at full field, H-mode access at $f_{\mathrm{GW}} = 0.5$ and full current is expected to be feasible, but maintaining H-mode at high density ($f_{\mathrm{GW}} = 0.9$) depends on the choice of D in the scaling.

Leaving the surface area as a free parameter or adding the plasma current as a fit parameter strongly increases the extrapolated threshold for ITER at 15 MA. It is good to note in this respect that the surface area and plasma current of ITER are outside the parameter range of the database, but as far as B_t, $\overline{n_e}$ and B_{pol} are concerned, the ITER operational space is an interpolation with regard to the database, thanks to the C-Mod data at high toroidal field and density. This is illustrated in figure 10 which shows the entire TC-26 database, rescaled over the TC-26 (B_t) scaling, except for the B_t and $\overline{n_e}$ dependence, versus those variables. The approximate

Table 5. Predictions of the L–H threshold power for ITER corresponding to the various scalings of table 4 at full field and current in deuterium at a density of 0.5 10^{20} m^{-3} and 1.0 10^{20} m^{-3}, and for SPARC in DT at full field and current at a density of 2.0 10^{20} m^{-3}.

Scaling	ITER pred. [MW] $n_e = 0.5\ 10^{20}$ m^{-3}	ITER pred. [MW] $n_e = 1.0\ 10^{20}$ m^{-3}	SPARC pred. [MW] $n_e = 2.0\ 10^{20}$ m^{-3}
ITPA 2008 (log-linear) [4]	52.3	86.0	21.8
ITPA 2008 (least-squares)	41.2	66.4	19.7
C-Mod only	44.0	94.1	13.0
AUG only	37.7	72.7	17.4
JET-ILW only	40.9 ($D = 1$)/70.6 ($D = 1.73$)	95.3 ($D = 1$)/165 ($D = 1.73$)	21.9 ($D = 1$)/37.9 ($D = 1.73$)
TC-26 (B_t)	**38.1 ($D = 1$)/73.5 ($D = 1.93$)**	**80.3 ($D = 1$)/155 ($D = 1.93$)**	**18.8 ($D = 1$)/36.3 ($D = 1.93$)**
TC-26 (B_t,S)	54.6 ($D = 1$)/98.6 ($D = 1.81$)	132 ($D = 1$)/238 ($D = 1.81$)	24.6 ($D = 1$)/44.5 ($D = 1.81$)
TC-26 (B_t,I_p)	61.0 ($D = 1$)/105 ($D = 1.73$)	142 ($D = 1$)/245 ($D = 1.73$)	27.4 ($D = 1$)/47.3 ($D = 1.73$)
TC-26 (B_{pol})	56.0 ($D = 1$)/93.3 ($D = 1.67$)	117 ($D = 1$)/196 ($D = 1.67$)	26.3 ($D = 1$)/43.8 ($D = 1.67$)
TC-26 (B_t.P_{sep})	33.3 ($D = 1$)/72.4 ($D = 2.17$)	70 ($D = 1$)/152 ($D = 2.17$)	18.6 ($D = 1$)/40.4 ($D = 2.17$)

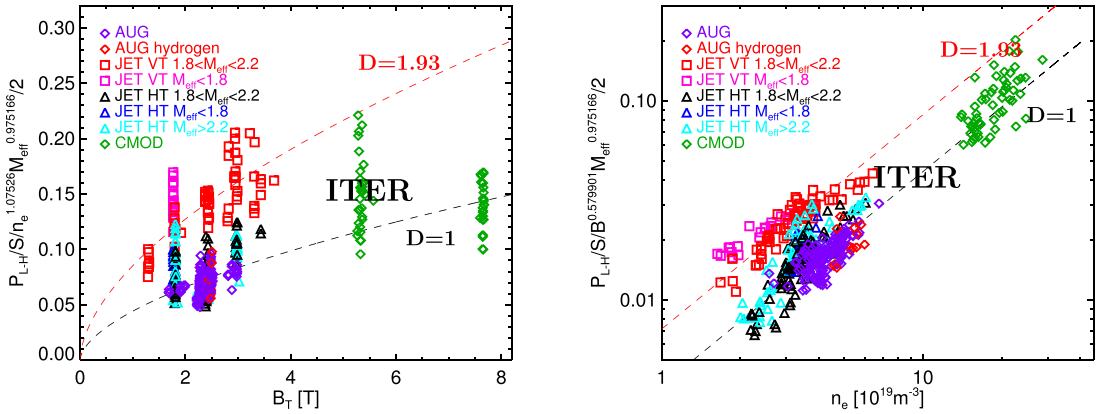

(a) Normalised data vs. B_t (b) Normalised data vs. $\overline{n_e}$

Figure 10. The TC-26 data rescaled over the TC-26 (B_t) scaling, except for a single variable. The approximate ITER operation point at full field and density is indicated. The dashed lines indicate the scalings for a HT-like divertor configuration ($D = 1$) and for a VT-like configuration ($D = 1.93$).

operational point for ITER at full field and density is overplotted. This also serves to show that the AUG data overlaps very well with the JET HT data once rescaled for size, despite AUG operating with the strike points on vertical targets, like ITER.

By contrast, application of these scalings to the SPARC tokamak (B_t = 8–12 T, n_e = 1–5 10^{20} m^{-3}) pushes towards and beyond the extremes of the TC-26 parameter range. L–H power thresholds for SPARC in both 12.2 T and 8.0 T scenarios were calculated according to both the 2008 ITPA scaling and the TC-26 (B_t) scaling, with $D = 1$ [48]. The newer TC-26 (B_t) scaling results in a reduced P_{L-H} projection at the proposed target density for H-mode entry. However the stronger density dependence of TC-26 (B_t) does introduce more challenging H-mode access at f_{GW} >0.4. Predictions for the threshold according to the various scalings presented here are shown in table 4 at full field and current at a density of n_e = 2 10^{20} m^{-3} in DT (using B_t = 12.2 T, I_p = 8.7 MA, $S = 58$ m^2). This is to be compared to an auxiliary heating power of 25 MW. SPARC presents a further opportunity to test the scalings explored here, and to provide additional constraints on projections for future burning plasma devices.

7. Discussion and outlook

This study highlights several uncertainties when extrapolating the L–H power threshold to future devices. The overarching uncertainty for any extrapolation based on these scalings is the effect of the divertor configuration within the JET data. It would be prudent to use the factor D as an indication of the maximum uncertainty range rather than the statistical uncertainties returned by the fit, as in [47]. It should however be noted that the $D = 1$ group aligns with data of three different devices and the higher D factor is derived from JET VT+CORNER data only and is thus considered anomalously high. The fact that ITER will operate with the strike points on the vertical targets does not necessarily mean the VT scaling is most ITER-like since AUG has a similar divertor shape to ITER and the C-Mod data in this database also has both strike points on the vertical targets, but they align with the JET HT configuration in terms of threshold.

Future experiments in metal wall devices aimed at elucidating the divertor configuration effect and the effect of the plasma current (or poloidal magnetic field) would be highest priority for narrowing down the uncertainties associated with the threshold scaling. This could include new insights from experiments with the upper divertor in AUG and potential experiments on EAST and KSTAR which have recently been fitted with tungsten divertors. Brief H-modes phases have been obtained in WEST [49] following boronization. The observed threshold of $P_{sep} = P_{L-H} - P_{rad} \approx 3$ MW at $\overline{n_e} \approx 5\ 10^{19}$ m^{-3} (figure 3 in [49]) is not inconsistent with the range predicted by the TC-26(B_t) scaling of $P_{L-H} = 2.46$ ($D = 1$) / 4 74 ($D = 1.9$) MW, using $B_t = 3.7$ T, $S = 54$ m^2 and $\overline{n_e} = 5\ 10^{19}$ m^{-3}. The TC-26(B_{pol}) scaling however would underestimate the threshold: $P_{L-H} = 1.45$ ($D = 1$) / 2.41 ($D = 1.7$) MW (for $I_p = 0.5$ MA, $a = 0.5$ m), assuming the transition is in the high density branch. The scaling for $n_{e,min}$ from [25] predicts $n_{e,min} = 4.6\ 10^{19}$m^{-3}, which is close to the density at which the L–H transitions are observed in [49].

8. Conclusions

New scalings for the H-mode power threshold for tokamaks with metallic plasma facing components have been derived as part of ITPA task TC-26 using data from AUG (W), JET (Be/W) and Alcator C-Mod (Mo). The database contains discharges in H, D and T as well as mixtures. An additional parameter was introduced to capture the difference in threshold on JET between discharges with the outer strike point on the HT or with both strike points on the vertical targets or in the divertor corners. The scalings are only valid for densities above the density for which the threshold has a minimum. The surface area exponent has been set to 1. Compared to the ITPA 2008 scaling [4], the metal wall TC-26 (B_t) scaling has a smaller magnetic field exponent. All TC-26 scalings have a larger density exponent and recover the $1/M_{eff}$ scaling with effective ion mass. The ca. 30% reduction in threshold seen on JET and AUG following the changeover to metallic plasma facing components does not extrapolate to a similar reduction of the threshold power on ITER, in particular at high density. At low densities and for a divertor configuration corresponding to the JET HT configuration group which also contains the AUG and C-Mod data, the TC-26 (B_t) scaling predicts a modest reduction in threshold for ITER, but the divertor configuration effect introduces a large uncertainty (factor ≈2) in the extrapolation. Note that the lower threshold group in the database contains data from three different devices and the higher D factor is derived from JET VT+CORNER data only and is as thus considered anomalously high. The fact that ITER will operate with the strike points on the vertical targets does not necessarily mean the VT scaling is most ITER-like since AUG has a similar divertor shape to ITER and the C-Mod data in this database also has both strike points on the vertical targets. Using B_{pol} in the scaling increases the predicted threshold for ITER. The TC-26 (B_{pol}) scaling tends to better align the data from the various machines. Additional experiments elucidating the effects of the divertor configuration and the plasma current on the H-mode threshold could help to narrow down the uncertainty in the extrapolation to future devices.

Acknowledgments

We would like to acknowledge the contributors to the C-Mod experimental program as well as the support of the ITPA Transport and Confinement group, in particular Darren McDonald and Knud Thomsen for originating this activity. Work supported, in part, by the US DOE under Contract No. DE-AC05-00OR22725 with UT-Battelle, LLC and under Award No. DE-SC0014264. This work was supported in part by Grants FIS2017-85252-R and PID2021-127727OB-I00 funded by the Spanish Ministry of Science, Innovation and Universities MICIU/AEI/10.13039/501100011033, by ERDF 'A way of making Europe' and by ERDF/EU. The project is co-funded by the national budget under the programme established by the Polish Minister of Science and Higher Education entitled 'Co-financed International Projects (PMW)'. This work has been carried out within the framework of the EUROfusion Consortium, funded by the European Union via the Euratom Research and Training Programme (Grant Agreement No. 101052200—EUROfusion). Views and opinions expressed are however those of the author(s) only and do not necessarily reflect those of the European Union or the European Commission. Neither the European Union nor the European Commission can be held responsible for them.

ORCID iDs

E. Delabie 0000-0001-9834-874X
E.R. Solano 0000-0002-4815-3407
J.W. Hughes 0000-0003-4802-4944
C.F. Maggi 0000-0001-7208-2613
G. Birkenmeier 0000-0001-7508-3646
P. Carvalho 0000-0002-8480-0499
M. Cavedon 0000-0002-0013-9753
M. Chernyshova 0000-0002-4149-0259
P. David 0000-0003-4837-8507
J. Hillesheim 0009-0009-5911-3417
U. Plank 0000-0002-1509-4308

References

[1] Loarte A. *et al* 2025 The new ITER baseline, research plan and open R&D issues *Plasma Phys. Control. Fusion* **67** 065023
[2] Suárez López G., Tardini G., Fable E., Siccinio M. and Zohm H. 2024 The feasibility of the L-H transition for a purely electron-heated EU-DEMO tokamak *Nucl. Fusion* **64** 126012
[3] Yoshida M. *et al* 2025 Transport and confinement physics: chapter 2 of the special issue: on the path to tokamak burning plasma operation *Nucl. Fusion* **65** 033001
[4] Martin Y.R. and Takizuka T. (the ITPA CDBM H-mode Threshold Database Working Group) 2008 Power requirement for accessing the H-mode in ITER *J. Phys.: Conf. Ser.* **123** 012033
[5] Ryter F. *et al* 1996 H mode power threshold database for ITER *Nucl. Fusion* **36** 1217

[6] The ITER H mode Threshold Database Working Group and presented by E Righi 1998 Scaling of the H-mode power threshold for ITER *Plasma Phys. Control. Fusion* **40** 857

[7] Snipes J.A. (the International H-mode Threshold Database Working Group) 2000 Latest results on the H-mode threshold using the international H-mode threshold database *Plasma Phys. Control. Fusion* **42** A299

[8] Ryter F. (the H-mode Threshold Database) Group 2002 Progress of the international H-mode power threshold database activity *Plasma Phys. Control. Fusion* **44** A415

[9] ITPA H mode Power Threshold Database Working Group presented by T Takizuka 2004 Roles of aspect ratio, absolute B and effective Z of the H-mode power threshold in tokamaks of the ITPA database *Plasma Phys. Control. Fusion* **46** A227

[10] Ryter F. *et al* 2013 Survey of the H-mode power threshold and transition physics studies in ASDEX Upgrade *Nucl. Fusion* **53** 113003

[11] Maggi C.F. *et al* 2014 L-H power threshold studies in JET with Be/W and C wall *Nucl. Fusion* **54** 023007

[12] Burrell K.H. 2020 Role of sheared E $\times$ B flow in self-organized, improved confinement states in magnetized plasmas *Phys. Plasmas* **27** 060501

[13] Plank U. *et al* 2023 Experimental study of the edge radial electric field in different drift configurations and its role in the access to H-mode at ASDEX Upgrade *Phys. Plasmas* **30** 042513

[14] Silva C., Solano E.R., Hillesheim J.C., Delabie E., Birkenmeier G., Gil L., Giroud C., Morales R.B. and Nina D. (JET Contributors) 2022 Effect of the divertor configuration on the JET edge radial electric field *Nucl. Fusion* **62** 126057

[15] Shao L.M., Wolfrum E., Ryter F., Birkenmeier G., Laggner F.M., Viezzer E., Fischer R., Willensdorfer M., Kurzan B. and Lunt T. (the ASDEX Upgrade Team) 2016 On the role of the edge density profile for the L-H transition power threshold in ASDEX Upgrade *Plasma Phys. Control. Fusion* **58** 025004

[16] Lunt T., Reimold F., Wolfrum E., Carralero D., Feng Y. and Schmid K. (the ASDEX Upgrade Team) 2017 Influence of the first wall material on the particle fuelling in ASDEX Upgrade *Plasma Phys. Control. Fusion* **59** 055016

[17] Maggi C.F. *et al* 2025 Impact of nitrogen injection on L-H transitions in JET with Be/W wall *Proc. of the 50th EPS Conf. on Plasma Physics* (*Salamanca, Spain, 2024*) (available at: www.ccm-events.com/epsplasma2024/imagenes/comunicaciones/2-Parallel_Session/0272-Maggi_EPS2024_abstract.pdf)

[18] Maggi C.F. 2014 Role of low-Z impurities in L-H transitions in JET *Proc. of the 41st EPS Conf. on Plasma Physics* (*Berlin, Germany, 2014*) (available at: http://ocs.ciemat.es/EPS2014PAP/pdf/P1.004.pdf)

[19] Delabie E. *et al* 2014 Overview and interpretation of L-H threshold experiments on JET with the ITER-like wall *25th IAEA Fusion Energy Conf.* (*Sain-Peterburg, Russia*, *2014*) (International Atomic Energy Agency IAEA) p EX/5–24 (available at: https://scipub.euro-fusion.org/wp-content/uploads/2015/04/EFDC140618.pdf)

[20] Bourdelle C. *et al* (JET EFDA Contributors) 2014 L to H mode transition: on the role of Zeff *Nucl. Fusion* **54** 022001

[21] Chankin A.V., Delabie E., Corrigan G., Harting D., Maggi C.F. and Meyer H. (JET Contributors) 2017 EDGE2D-EIRENE modelling of near SOL E_r: possible impact on the H-mode power threshold *Plasma Phys. Control. Fusion* **59** 045012

[22] Plank U. *et al* (the ASDEX Upgrade Team) 2022 Overview of L- to H-mode transition experiments at ASDEX Upgrade *Plasma Phys. Control. Fusion* **65** 014001

[23] Ryter F. *et al* (the ASDEX Upgrade Team) 2015 L-H transition physics in hydrogen and deuterium: key role of the edge radial electric field and ion heat flux *Plasma Phys. Control. Fusion* **58** 014007

[24] Plank U. *et al* 2020 H-mode power threshold studies in mixed ion species plasmas at ASDEX Upgrade *Nucl. Fusion* **60** 074001

[25] Ryter F., Orte L.B., Kurzan B., McDermott R.M., Tardini G., Viezzer E., Bernert M. and Fischer R. (The ASDEX Upgrade Team) 2014 Experimental evidence for the key role of the ion heat channel in the physics of the L-H transition *Nucl. Fusion* **54** 083003

[26] Cavedon M. *et al* 2020 Connecting the global H-mode power threshold to the local radial electric field at ASDEX Upgrade *Nucl. Fusion* **60** 066026

[27] Ma Y., Hughes J.W., Hubbard A.E., LaBombard B., Churchill R.M., Golfinopolous T., Tsujii N. and Marmar E.S. 2012 Scaling of H-mode threshold power and L-H edge conditions with favourable ion grad-B drift in Alcator C-Mod tokamak *Nucl. Fusion* **52** 023010

[28] Tolman E.A., Hughes J.W., Wolfe S.M., Wukitch S.J., LaBombard B., Hubbard A.E., Marmar E.S., Snyder P.B. and Schmidtmayr M. 2018 Influence of high magnetic field on access to stationary H-modes and pedestal characteristics in Alcator C-Mod *Nucl. Fusion* **58** 046004

[29] Schmidtmayr M. *et al* 2018 Investigation of the critical edge ion heat flux for L-H transitions in Alcator C-Mod and its dependence on B_T *Nucl. Fusion* **58** 056003

[30] Ma Y., Hughes J.W., Hubbard A.E., LaBombard B. and Terry J. 2012 H-mode power threshold reduction in a slot-divertor configuration on the Alcator C-Mod tokamak *Plasma Phys. Control. Fusion* **54** 082002

[31] Solano E.R. *et al* 2022 Recent progress in L-H transition studies at JET: tritium, helium, hydrogen and deuterium *Nucl. Fusion* **62** 076026

[32] Solano E.R. *et al* 2023 L-H transition studies in tritium and deuterium-tritium campaigns at JET with be wall and W divertor *Nucl. Fusion* **63** 112011

[33] Andrew Y. *et al* 2004 JET divertor geometry and plasma shape effects on the L-H transition threshold *Plasma Phys. Control. Fusion* **46** A87

[34] Solano E.R. *et al* 2021 L-H transition threshold studies in helium plasmas at JET *Nucl. Fusion* **61** 124001

[35] Delabie E. *et al* 2015 The relation between divertor conditions and the L-H threshold on JET *Proc. of the 42nd EPS Conf. on Plasma Physics (Lisbon)* (*Lisbon, Portugal, 2015*) (available at: http://ocs.ciemat.es/EPS2015PAP/pdf/O3.113.pdf)

[36] Hillesheim J. *et al* 2017 L-H transition studies in hydrogen and mixed ion species plasmas in JET *44th EPS Conf. on Plasma Physics (Belfast)* p 5.162

[37] Maggi C.F. *et al* 2017 Isotope effects on L-H threshold and confinement in tokamak plasmas *Plasma Phys. Control. Fusion* **60** 014045

[38] Birkenmeier G. *et al* 2022 The power threshold of H-mode access in mixed hydrogen-tritium and pure tritium plasmas at JET with ITER-like wall *Nucl. Fusion* **62** 086005

[39] Birkenmeier G. *et al* 2023 The role of isotope mass and transport for H-mode access in tritium containing plasmas at JET with ITER-like wall *Plasma Phys. Control. Fusion* **65** 054001

[40] Garzotti L. *et al* 2025 Development of high-current baseline scenario for high deuterium-tritium fusion performance at JET *Plasma Phys. Control. Fusion* **67** 075011

[41] Arshad S., Budny R., Cordey J.G., Drozdov V., Gerasimov S., McDonald D.C., Murari A., Riccardo V. and Voitsekhovich I. (JET EFDA Contributors) 2005 Consistency of stored energy measurements on JET *Technical Report* EFDA-JET-CP (05) 02–50

[42] Righi E. *et al* 1999 Isotope scaling of the H mode power threshold on JET *Nucl. Fusion* **39** 309
[43] Reinke M.L. and Hutchinson I.H. 2008 Two dimensional radiated power diagnostics on Alcator C-Mod *Rev. Sci. Instrum.* **79** 10F306
[44] David P., Bernert M., Pütterich T., Fuchs C., Glöggler S. and Eich T. (the ASDEX Upgrade Team) 2021 Optimization of the computation of total and local radiated power at ASDEX Upgrade *Nucl. Fusion* **61** 066025
[45] Bilato R., Angioni C., Birkenmeier G. and Ryter F. (ASDEX Upgrade Team) 2020 Heuristic model for the power threshold of the L-H transition *Nucl. Fusion* **60** 124003
[46] Loarte A. *et al* 2021 H-mode plasmas in the pre-fusion power operation 1 phase of the ITER research plan *Nucl. Fusion* **61** 076012
[47] Vincenzi P., Delabie E., Loarte A., Schneider M., Solano E.R. and Contributors J.E.T. 2025 Connecting recent JET isotope L-H transition studies to H-mode access in new ITER scenarios *Plasma Phys. Control. Fusion* **67** 045013
[48] Hughes J.W. *et al* 2025 High confinement regimes on SPARC: operational conditions for access and avoidance *Nucl. Fusion* **65** 052001
[49] Vermare L. *et al* 2021 Formation of the radial electric field profile in the WEST tokamak *Nucl. Fusion* **62** 026002